Current Optics and Photonics
Vol. 3, No. 4, August 2019, pp. 342-349

ISSN: 2508-7266(Print) / ISSN: 2508-7274(Online)
DOI: https://doi.org/10.3807/COPP.2019.3.4.342

Theoretical Investigation on Collinear Phase Matching Stimulated Polariton Scattering Generating THz Waves with a KTP Crystal

Lian Tan[1], Bin Yuan[1], Yongjun Li[1], Silei Wang[1], Hongtao Zhang[1], Pibin Bing[1], Jianquan Yao[2], and Zhongyang Li[1]*

[1]College of Electric Power, North China University of Water Resources and Electric Power, Zhengzhou 450045, China
[2]College of Precision Instrument and Opto-electronics Engineering, Institute of Laser and Opto-electronics, Tianjin University, Tianjin, 300072, China

(Received February 28, 2019 : revised May 12, 2019 : accepted May 24, 2019)

We present a theoretical research concerning terahertz (THz) wave generation with $KTiOPO_4$ (KTP) by collinear phase matching (CPM) stimulated polariton scattering (SPS). Both CPM and corresponding nonzero nonlinear coefficients can be simultaneously realized with $s \rightarrow f+f$ in yz plane, $s \rightarrow f+s$ with $\theta < \Omega$ in xz plane and $s \rightarrow f+f$ with $\theta > \Omega$ in xz plane. The effective nonlinear coefficients including electronic nonlinearities and ionic nonlinearities are calculated. Based on the parameter values of refractive indices, absorption coefficients and effective nonlinear coefficients, we simulate THz wave intensities generated with CPM SPS by solving coupled wave equations and give the relationship among the maximum THz wave intensity, optimal crystal length and the angle θ. The calculation results demonstrate that CPM SPS with KTP can generate THz waves with high intensities and quantum conversion efficiencies.

Keywords : Terahertz wave, Stimulated polariton scattering, $KTiOPO_4$
OCIS codes : (190.4410) Nonlinear optics, parametric processes; (190.4223) Nonlinear wave mixing

I. INTRODUCTION

Over the past two decades, stimulated polariton scattering (SPS) has proven to be an efficient scheme to generate terahertz (THz) waves [1-4] because SPS can stimulate both electronic and ionic nonlinearities [5, 6]. To realize high-power THz radiations, the nonlinear crystal must possess low absorption coefficients at THz frequencies, large effective nonlinear coefficients and a high optical damage threshold. In addition, it is advantageous for the crystal to have low refractive indices at THz frequencies to allow collinear phase matching (CPM) during SPS processes. $MgO:LiNbO_3$ has been the most widely used crystal for THz wave generation via SPS [7-9]. Due to strong dispersion of $MgO:LiNbO_3$ between the optical and THz frequencies, CPM cannot be realized [1]. Moreover, because of large absorption coefficients at THz frequencies, the tuning range of THz waves is 0.5~3.2 THz.

$KTiOPO_4$ (KTP) is one of the most widely used nonlinear optical crystals for optical frequency conversion. KTP belongs to the *mm*2 point group symmetry and its dielectric and crystallographic axes are assigned as x, y, z $\rightarrow$ a, b, c. Advantages of KTP are moderate nonlinear coefficients: $d_{15} = 1.9$ pm/V, $d_{24} = 3.7$ pm/V, $d_{31} = 2.2$ pm/V, $d_{32} = 3.7$ pm/V and $d_{33} = 14.6$ pm/V [10], wide transparency range from 0.35 μm to 4.5 μm with "0" level [11], high optical damage threshold of over 30 GW/cm^2 at 1064 nm with 8~11 ns pulse [10], excellent mechanical stability and high optical quality. KTP is an excellent nonlinear crystal for sum frequency generation [12], difference frequency generation [13], and optical parametric oscillation [14] generating visible, near-infrared and mid-infrared waves. Moreover, KTP is also an attractive crystal for THz generation [15-17]. KTP has four very intense infrared- and

*Corresponding author: thzwave@163.com, ORCID 0000-0001-8350-5781

Color versions of one or more of the figures in this paper are available online.

Raman-active A_1 transverse optical (TO) phonon modes, which are located at 268.5, 311, 385 and 687 cm^{-1}, and the lowest mode (268.5 cm^{-1}) is useful for efficient tunable THz wave generation because of the largest parametric gain, as well as the smallest absorption coefficient [18]. THz wave generation with SPS in KTP shows superior performance in terms of parametric gain and laser damage resistance in comparison to $LiNbO_3$ and $LiTaO_3$ [15].

In the reported works, THz waves were generated experimentally from SPS with KTP by noncollinear phase matching schemes [15-17]. The noncollinear phase matching configuration restricts the interaction volume among mixing waves, as a result, the quantum conversion efficiency from pump waves to THz waves is low. Huang *et al.* measured the KTP refractive index in the range of 142~1500 μm at room temperature [19]. They investigated CPM conditions of difference frequency generation for down-conversion into the THz range under a visible and near infrared pump wave with KTP. In this work, we theoretically investigate THz wave generation with KTP by CPM SPS. We deduce the expression of absorption coefficients for THz waves. CPM conditions of SPS are analyzed. We calculate effective nonlinear coefficients involved in SPS processes. Based on the parameters above, we calculate the intensities of THz waves by solving coupled wave equations.

II. ABSORPTION COEFFICIENTS OF THz WAVES

The relationship between propagation constant $\vec{k}$, electric field strength $\vec{E}$ and electric displacement vector $\vec{D}$ is written as

$$\mu_0\omega^2\vec{D}=\left[k^2\vec{E}-\left(\vec{k}\cdot\vec{E}\right)\vec{k}\right] \tag{1}$$

where μ_0 is permeability of vacuum and ω is angular frequency. $\vec{k}=\vec{k}_r+i\vec{k}_i$, $\vec{k}_r$ relates to dispersion and $\vec{k}_i$ relates to material absorption. $\vec{D}=\vec{\varepsilon}\cdot\vec{E}$, where dielectric constant $\vec{\varepsilon}=\vec{\varepsilon}_r+i\vec{\varepsilon}_i$. The propagation constant $\vec{k}$ along the principal axes x, y, z is $k_1=k\sin\theta\cos\varphi$, $k_2=k\sin\theta\sin\varphi$, and $k_3=k\cos\theta$, respectively. Here, θ is the angle between the wave vector and the z axis, φ is the angle from the x axis in the xy plane. The Eq. (1) is divided into the following two equations,

$$\mu_0\omega^2\vec{D}_r=\left[k_r^2\vec{E}-\left(\vec{k}_r\cdot\vec{E}\right)\vec{k}_r\right] \tag{2}$$

$$\mu_0\omega^2\vec{D}_i=\left[k_i^2\vec{E}-\left(\vec{k}_i\cdot\vec{E}\right)\vec{k}_i\right] \tag{3}$$

where k_0 is wave vector at vacuum, $\vec{D}_r=\vec{\varepsilon}_r\cdot\vec{E}$ and $\vec{D}_i=\vec{\varepsilon}_i\cdot\vec{E}$. As Eq. (3) relates to material absorption, we deduce the expressions of material absorption from Eq. (3). In the principal axis coordinate system, ε_i is given by

$$\varepsilon_i=\begin{pmatrix}\varepsilon_{i1} & 0 & 0\\ 0 & \varepsilon_{i2} & 0\\ 0 & 0 & \varepsilon_{i3}\end{pmatrix} \tag{4}$$

$$\begin{pmatrix}D_{i1}\\ D_{i2}\\ D_{i3}\end{pmatrix}=\begin{pmatrix}\varepsilon_{i1} & 0 & 0\\ 0 & \varepsilon_{i2} & 0\\ 0 & 0 & \varepsilon_{i3}\end{pmatrix}\begin{pmatrix}E_1\\ E_2\\ E_3\end{pmatrix}=\begin{pmatrix}\varepsilon_{i1}E_1\\ \varepsilon_{i2}E_2\\ \varepsilon_{i3}E_3\end{pmatrix} \tag{5}$$

According to Eqs. (3)~(5), Eq. (3) can be rewritten as

$$\begin{aligned}&k_i^2\left(k_{i1}^2\varepsilon_{i1}+k_{i2}^2\varepsilon_{i2}+k_{i3}^2\varepsilon_{i3}\right)+\mu_0{}^2k_0^4c^4\varepsilon_{i1}\varepsilon_{i2}\varepsilon_{i3}\\&-\mu_0k_0^2c^2\left[\varepsilon_{i1}k_{i1}^2\left(\varepsilon_{i2}+\varepsilon_{i3}\right)+\varepsilon_{i2}k_{i2}^2\left(\varepsilon_{i1}+\varepsilon_{i3}\right)+\varepsilon_3k_{i3}^2\left(\varepsilon_{i1}+\varepsilon_{i2}\right)\right]=0\end{aligned} \tag{6}$$

In the xy plane of a biaxial crystal, $k_{i3}=0$, the two solutions of Eq. (6) are

$$k'_{ixy}=\sqrt{\varepsilon_{i3}}k_0 \tag{7a}$$

$$k''_{ixy}=k_0\left(\frac{\sin^2\varphi}{\varepsilon_{i1}}+\frac{\cos^2\varphi}{\varepsilon_{i2}}\right)^{-\frac{1}{2}} \tag{7b}$$

In the yz plane of a biaxial crystal, $k_{i1}=0$, the two solutions of Eq. (6) are

$$k'_{iyz}=\sqrt{\varepsilon_{i1}}k_0 \tag{8a}$$

$$k''_{iyz}=k_0\left(\frac{\sin^2\left(90^\circ-\theta\right)}{\varepsilon_{i2}}+\frac{\cos^2\left(90^\circ-\theta\right)}{\varepsilon_{i3}}\right)^{-\frac{1}{2}} \tag{8b}$$

In the xz plane of a biaxial crystal, $k_{i2}=0$, the two solutions of Eq. (6) are

$$k'_{ixz}=\sqrt{\varepsilon_{i2}}k_0 \tag{9a}$$

$$k''_{ixz}=k_0\left(\frac{\sin^2\theta}{\varepsilon_{i3}}+\frac{\cos^2\theta}{\varepsilon_{i1}}\right)^{-\frac{1}{2}} \tag{9b}$$

Because k_i and ε_i relate to material absorption, Eqs. (7)~(9) can be rewritten as

$$\alpha'_{xy}=\alpha_z \tag{10a}$$

$$\alpha''_{xy}=\left(\frac{\sin^2\varphi}{\alpha_x^2}+\frac{\cos^2\varphi}{\alpha_y^2}\right)^{-\frac{1}{2}} \tag{10b}$$

$$\alpha'_{yz} = \alpha_x \tag{11a}$$

$$\alpha''_{yz} = \left(\frac{\sin^2(90^\circ - \theta)}{\alpha_y^2} + \frac{\cos^2(90^\circ - \theta)}{\alpha_z^2} \right)^{-\frac{1}{2}} \tag{11b}$$

$$\alpha'_{xz} = \alpha_y \tag{12a}$$

$$\alpha''_{xz} = \left(\frac{\sin^2\theta}{\alpha_z^2} + \frac{\cos^2\theta}{\alpha_x^2} \right)^{-\frac{1}{2}} \tag{12b}$$

where α''_{xy}, α''_{yz} and α''_{xz} are material absorption coefficients at *xy*, *yz* and *xz* planes, respectively, α'_{xy}, α'_{yz} and α'_{xz} are absorption coefficients with polarization direction along *z*, *x* and *y* axes, respectively.

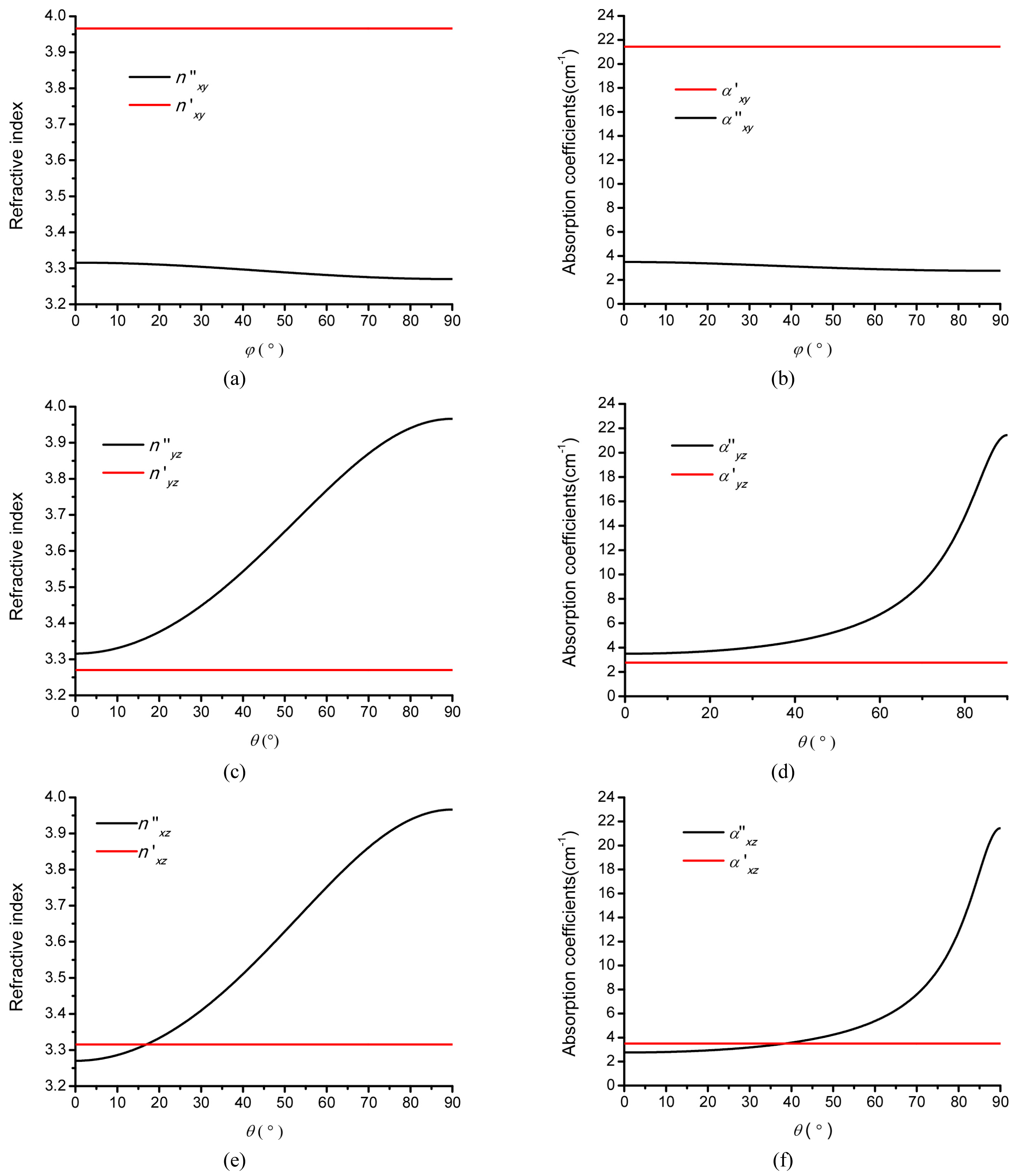

FIG. 1. Refractive indices and absorption coefficients of a THz wave at 1 THz. (a) and (b) *xy* plane, (c) and (d) *yz* plane, (e) and (f) *xz* plane.

Because Eqs. (2) and (3) have the same form, the expressions of refractive indices are given by,

$$n'_{xy}=n_z \tag{13a}$$

$$n''_{xy}=\left(\frac{\sin^2\varphi}{n_x^2}+\frac{\cos^2\varphi}{n_y^2}\right)^{-\frac{1}{2}} \tag{13b}$$

$$n'_{yz}=n_x \tag{14a}$$

$$n''_{yz}=\left(\frac{\sin^2\left(90^\circ-\theta\right)}{n_y^2}+\frac{\cos^2\left(90^\circ-\theta\right)}{n_z^2}\right)^{-\frac{1}{2}} \tag{14b}$$

$$n'_{xz}=n_y \tag{15a}$$

$$n''_{xz}=\left(\frac{\sin^2\theta}{n_z^2}+\frac{\cos^2\theta}{n_x^2}\right)^{-\frac{1}{2}} \tag{15b}$$

where n''_{xy}, n''_{yz} and n''_{xz} are refractive indices in *xy*, *yz* and *xz* plane, respectively, n'_{xy}, n'_{yz} and n'_{xz} are refractive indices with polarization direction along *z*, *x* and *y* axis, respectively. The analytical expressions of α''_{xy}, α''_{yz}, α''_{xz}, α'_{xy}, α'_{yz} and α'_{xz} have the same form with those of n''_{xy}, n''_{yz}, n''_{xz}, n'_{xy}, n'_{yz} and n'_{xz}, respectively, where n''_{xy}, n''_{yz} and n''_{xz} are refractive indices in *xy*, *yz* and *xz* planes, respectively, n'_{xy}, n'_{yz} and n'_{xz} are refractive indices with polarization direction along *z*, *x* and *y* axes, respectively [20]. Figure 1 shows refractive indices and absorption coefficients of a THz wave at 1 THz. The theoretical values of the refractive index are calculated using a Sellmeier equation for KTP in the infrared range [21] and THz range [19], respectively. As the Sellmeier equation for a THz wave is applicable in the range of 0.2~2.1 THz, in this work we calculate phase matching conditions and THz intensities in this range. Absorption coefficients of a THz wave for high-resistivity KTP with polarization direction along *x*, *y* and *z* axes are reported by Antsygin *et al.* [22]. From the figure we find that refractive indices and absorption coefficients vary with a same trend. In *xy* plane, n''_{xy} and α''_{xy} decrease smoothly with φ. In *yz* and *xz* plane, n''_{yz}, n''_{xz}, α''_{yz} and α''_{xz} increase smoothly and rapidly with θ.

III. PHASE-MATCHING CHARACTERISTICS

CPM and large nonlinear coefficients for SPS generating THz waves are preferred. Table 1 shows CPM conditions and the corresponding nonlinear coefficients for KTP. The CPM conditions in Table 1 are derived from an energy conservation condition and a momentum conservation condition among three mixing waves. The nonlinear coefficients in Table 1 are derived from the wave vectors and polarizations of the three mixing waves. As the refractive indices in THz range are larger than those in infrared range, CPM can hardly be satisfied. CPM cannot be satisfied with type-0 phase matching *s*→*s*+*s* in *yz* and *xz* planes which utilizes the maximum nonlinear coefficient d_{33}. *s* denotes slow light. Only three situations can realize both CPM and the corresponding nonzero nonlinear coefficient, *s*→*f*+*f* in the *yz* plane, *s*→*f*+*s* with $\theta<\Omega$ and *s*→*f*+*f* with

TABLE 1. CPM conditions and the corresponding nonlinear coefficients for KTP with pump wavelength of 1.064 μm. Y indicates CPM can satisfy, and N indicates CPM cannot satisfy

xy plane	*f*→*f*+*s*		nonzero	N
	f→*s*+*f*		nonzero	N
	f→*s*+*s*		0	N
	f→*f*+*f*		0	N
	s→*f*+*s*		0	N
	s→*s*+*f*		0	N
	s→*s*+*s*		nonzero	N
	s→*f*+*f*		nonzero	N
yz plane	*s*→*f*+*f*		nonzero	Y
	s→*f*+*s*		0	Y
	s→*s*+*s*		nonzero	N
	s→*s*+*f*		0	N
	f→*f*+*f*		0	N
	f→*f*+*s*		nonzero	N
	f→*s*+*f*		nonzero	N
	f→*s*+*s*		0	N
xz plane	*f*→*s*+*s*	$\theta<\Omega$	nonzero	N
		$\theta>\Omega$	0	N
	f→*f*+*s*	$\theta<\Omega$	0	N
		$\theta>\Omega$	nonzero	N
	f→*s*+*f*	$\theta<\Omega$	0	N
		$\theta>\Omega$	nonzero	N
	f→*f*+*f*	$\theta<\Omega$	nonzero	N
		$\theta>\Omega$	0	N
	s→*s*+*s*	$\theta<\Omega$	0	N
		$\theta>\Omega$	nonzero	N
	s→*f*+*s*	$\theta<\Omega$	nonzero	Y
		$\theta>\Omega$	0	Y
	s→*s*+*f*	$\theta<\Omega$	nonzero	N
		$\theta>\Omega$	0	N
	s→*f*+*f*	$\theta<\Omega$	0	Y
		$\theta>\Omega$	nonzero	Y

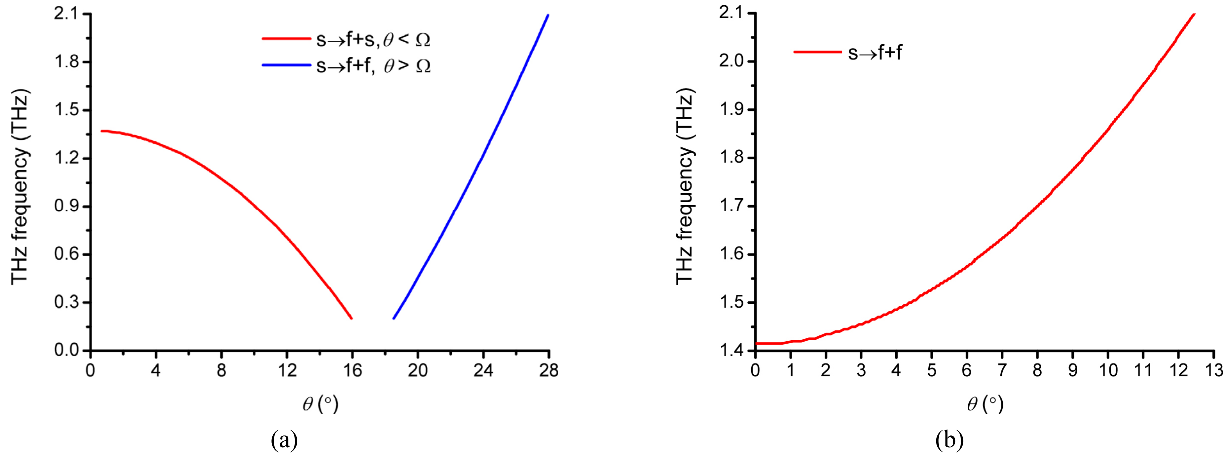

FIG. 2. THz frequencies versus θ with CPM for KTP with a pump wavelength of 1.064 μm. (a) *s→f+s* with $\theta<\Omega$ and *s→f+f* with $\theta>\Omega$ in the *xz* plane, (b) *s→f+f* in the *yz* plane.

$\theta>\Omega$ in the *xz* plane. *f* denotes fast light, and Ω denotes optic axial angle. Figure 2 shows THz frequencies versus θ with CPM for KTP with a pump wavelength of 1.064 μm. In the *xz* plane *s→f+s* with $\theta<\Omega$, THz waves with frequencies from 0.2 to 1.37 THz are generated with θ from 0.7° to 16°. The THz frequencies decrease slowly and then fast with θ. In the *xz* plane *s→f+f* with $\theta>\Omega$, THz waves with frequencies from 0.2 to 2.1 THz are generated with θ from 18.5° to 28°. The THz frequencies increase rapidly with θ. In the *yz* plane *s→f+f*, THz waves with frequencies from 1.42 to 2.1 THz are generated with θ from 0° to 12.5°. The THz frequencies increase smoothly and then fast with θ. The above three CPM schemes are suitable for THz wave generation because all the absorption coefficients of the THz waves are α'_{yz} and α'_{xz} with low values.

IV. NONLINEAR OPTICAL COEFFICIENTS

Nonlinear optical coefficients are purely electronic when frequencies of the mixing waves involved in SPS are far above the TO mode frequencies. However, when the frequencies of THz waves are near the TO mode frequencies, ionic nonlinearities as well as electronic nonlinearities are present. The bulk nonlinear coefficient db for SPS for KTP are written as follows [3, 5]:

$$d_b = d_e + \frac{S_0\omega_0^2}{\omega_0^2-\omega_T^2-i\Gamma_0\omega_T}d_Q \tag{16}$$

where d_e is the electronic second-order nonlinear coefficient, d_Q is the ionic third-order nonlinear coefficient. d_b is the bulk value of the nonlinear coefficient involving electronic and ionic contributions. ω_0, S_0 and Γ_0 denote eigenfrequency, oscillator strength and bandwidth of the TO mode, respectively. ω_T is the angular frequency of the THz wave. Since we are interested only in the lowest intense polariton branch 268.5 cm^{-1}, high frequency TO modes are not considered in Eq. (16) [3, 5]. With ω_0 of 268.5 cm^{-1}, S_0 is 2.5 and Γ_0 is 4.5 cm^{-1}. d_e is d_{31} in *yz* plane, whereas d_e is d_{24} in the *xz* plane. Jang *et al.* estimate that the value of d_Q is 183 pm/V [3]. The effective nonlinear coefficient d_{eff} for *s→f+s* with $\theta<\Omega$ and *s→f+f* with $\theta>\Omega$ in the *xz* plane is given by

$$d_{eff} = d_b \sin\theta \tag{17}$$

Figure 3 shows the effective nonlinear coefficient d_{eff} versus THz frequencies by a pump wavelength of 1.064 μm with θ of 5°, 30°, 45°, 60° and 90°. d_{eff} increases smoothly with THz frequencies. When frequencies approach the lowest TO mode of 268.5 cm^{-1}, ionic nonlinearities which are described by Eq. (16) are enhanced. When θ changes from 5° to 30°, 45°, 60° and 90°, d_{eff} increases obviously.

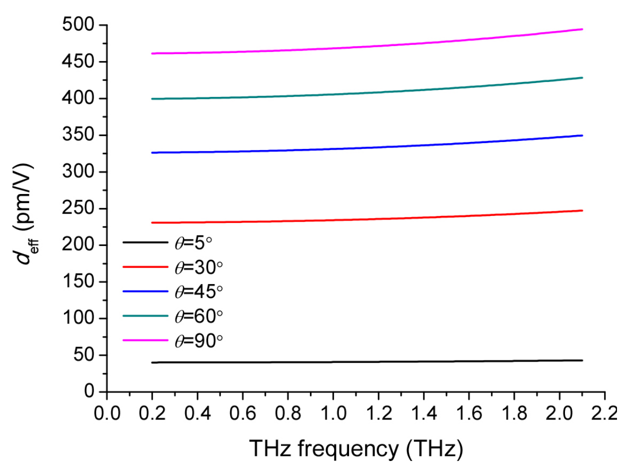

FIG. 3. The effective nonlinear coefficient deff versus THz frequencies by a pump wavelength of 1.064 μm with θ of 5°, 30°, 45°, 60° and 90°.

V. INTENSITIES OF THz WAVES

In this section, we calculate intensities of THz waves for *s→f+s* with $\theta<\Omega$ and *s→f+f* with $\theta>\Omega$ in the *xz* plane. In SPS processes, we assume that the pump, Stokes and THz waves are continuous plane waves with slowly varying envelopes co-propagating along the +ξ direction. Under the slowly varying approximation, the coupled-wave equations for CPM SPS processes are written as

$$\frac{\partial \vec{E}_{\rm p}}{\partial \xi}=-i\kappa_{\rm p}\vec{E}_{\rm s}\vec{E}_{\rm T}e^{i\Delta k\xi} \tag{18}$$

$$\frac{\partial \vec{E}_{\rm s}}{\partial \xi}=-i\kappa_{\rm s}\vec{E}_{\rm p}\vec{E}_{\rm T}^{*}e^{-i\Delta k\xi} \tag{19}$$

$$\frac{\partial \vec{E}_{\rm T}}{\partial \xi}=-\frac{\alpha_{\rm T}}{2}\vec{E}_{\rm T}-i\kappa_{\rm T}\vec{E}_{\rm p}\vec{E}_{\rm s}^{*}e^{-i\Delta k\xi} \tag{20}$$

$$\kappa_{\rm p}=\frac{\omega_{\rm p}d_{\rm eff}}{cn_{\rm p}} \tag{21}$$

$$\kappa_{\rm s}=\frac{\omega_{\rm s}d_{\rm eff}}{cn_{\rm s}} \tag{22}$$

$$\kappa_{\rm T}=\frac{\omega_{\rm T}d_{\rm eff}}{cn_{\rm T}} \tag{23}$$

where Δk is phase mismatch, $n_{\rm p}$, $n_{\rm s}$ and $n_{\rm T}$ are refractive indices of pump, Stokes and THz waves, respectively, $\omega_{\rm p}$, $\omega_{\rm s}$ and $\omega_{\rm T}$ are angular frequencies of pump, Stokes and THz waves, respectively, $\kappa_{\rm p}$, $\kappa_{\rm s}$ and $\kappa_{\rm T}$ are coupling coefficients of pump, Stokes and THz waves, respectively. $\alpha_{\rm T}$ is the absorption coefficient of the THz wave along the +ξ direction. With THz wave absorption, without phase mismatch and pump depletion, the coupled wave equations can be solved to give THz intensities, as shown in Fig. 4. In the calculations pump wave intensity $I_{\rm p}=10$ MW/mm², initial Stokes wave intensity $I_{\rm s}=10$ W/mm². With a pump wavelength of 1.064 μm and θ of 5°, 10°, 15°, 21°, 24° and 27°, the generated THz frequencies are 1.26, 0.9, 0.33, 0.64, 1.23 and 1.87 THz in the *xz* plane, respectively. The maximum intensities are 0.016, 0.021 and 0.009 MW/mm² when θ is 5°, 10° and 15°, respectively, corresponding to the quantum conversion efficiencies of 35%, 66.7% and 76.9% and optimal crystal length of 23.1 mm, 12.0 mm, 13.1 mm, respectively. The quantum conversion efficiency with θ of 5°is larger than those with θ of 10° and 15° because the SPS process with θ of 5° has the larger effective nonlinear coefficient and lower THz absorption coefficient. The maximum intensities are 0.019, 0.035 and 0.032 MW/mm² when θ is 21°, 24° and 27° respectively, corresponding to the quantum conversion efficiencies of 83.7%, 79.3% and 47.8%, and optimal crystal length of 6.7 mm, 4.2 mm, and 3.3 mm, respectively. With a pump wavelength of 1.064 μm and θ of 4°, 8° and 12°, the generated THz frequencies are 1.49, 1.7, and 2.06 THz in the *yz* plane, respectively. The maximum intensities are 0.013, 0.020 and 0.009 MW/mm² when θ is 4°, 8° and 12°, respectively, corresponding to the quantum conversion efficiencies of 24.6%, 33.7% and 12.4% and optimal crystal length of 28.3 mm, 12.3 mm, 9.5 mm, respectively. The quantum conversion efficiency with θ of 12° is small because absorption coefficient of 2.06 THz is too large with θ of 12°.

Figure 5 shows the relationship among the maximum THz wave intensity, the optimal crystal length and the angle θ with a pump wavelength of 1.064 μm. In the calculations pump wave intensity $I_{\rm p}=10$ MW/mm², initial Stokes wave intensity $I_{\rm s}=10$ W/mm². The intensities increase to the maximum value first and then decrease with the angle θ, and the optimal crystal lengths decrease fast and smoothly with the angle θ for *s→f+f* in *yz* plane, *s→f+s* with $\theta<\Omega$ in the *xz* plane and *s→f+f* with $\theta>\Omega$ in the *xz* plane. The most intense THz intensity of 0.043 MW/mm² can be generated for *s→f+f* in the *xz* plane with θ of 26° and crystal length of 2.44 mm, corresponding to the quantum conversion efficiencies of 73%.

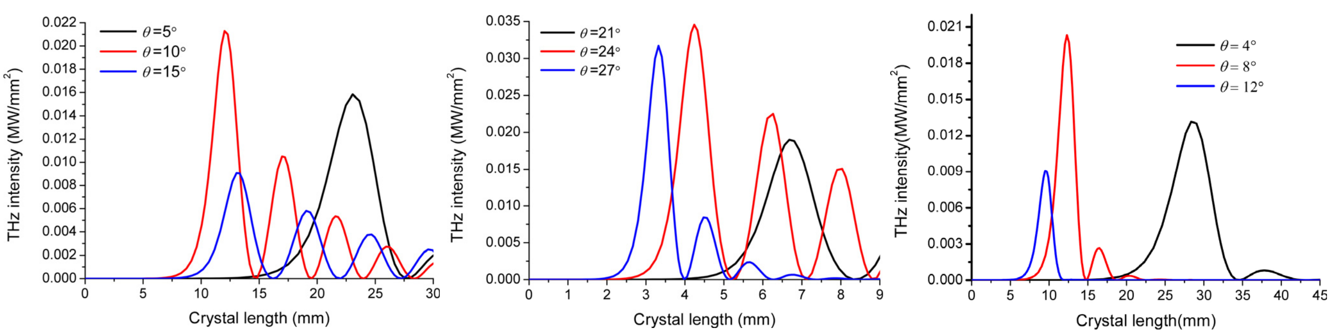

(a) (b) (c)

FIG. 4. THz wave intensities versus crystal length with a pump wavelength of 1.064 μm. Pump intensity Ip = 10 MW/mm², initial Stokes intensity Is = 10 W/mm². (a) s→f+s with θ < Ω in the xz plane, θ = 5°, 10° and 15°, (b) s→f+f with θ > Ω in the xz plane, θ = 21°, 24° and 27°, (c) s→f+f in the yz plane, θ = 4°, 8° and 12°.

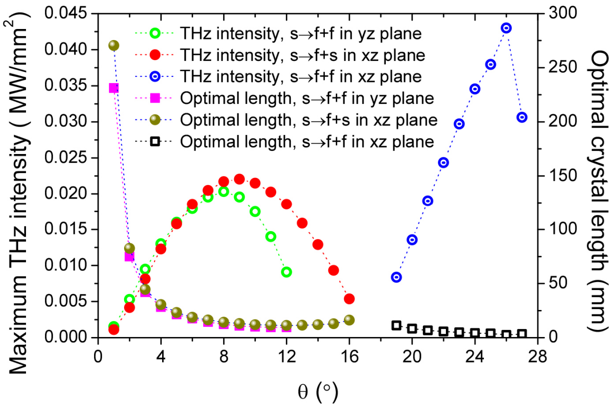

FIG. 5. The maximum THz wave intensity and optimal crystal length versus the angle θ with a pump wavelength of 1.064 μm. Pump intensity $I_p = 10$ MW/mm^2, initial Stokes intensity $I_s = 10$ W/mm^2.

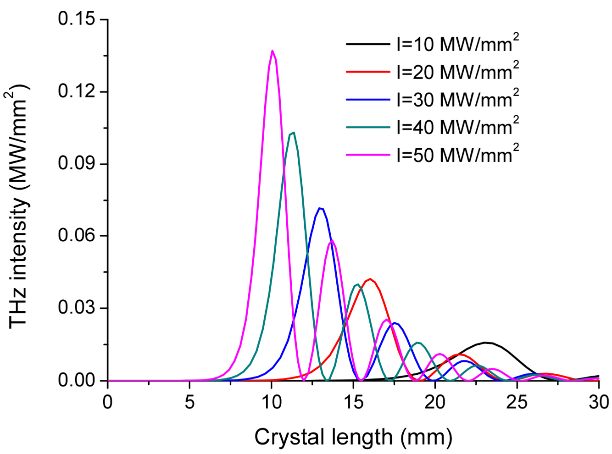

FIG. 6. THz wave intensities versus crystal length for $s \to f+f$ in the xz plane with a pump wavelength of 1.064 μm and θ of 5°. Pump intensity $I_p = 10$, 20, 30, 40 and 50 MW/mm^2, initial Stokes intensities $I_s = 10$ W/mm^2.

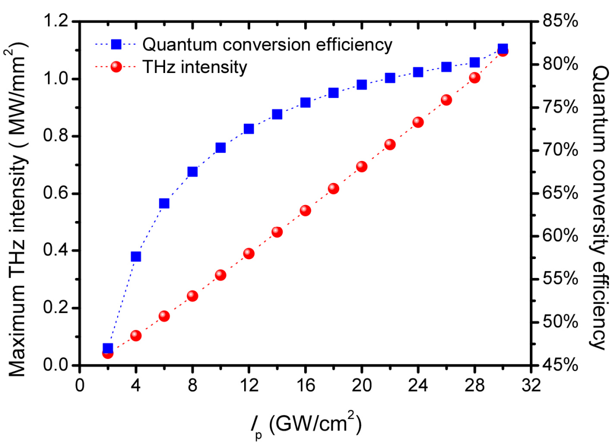

FIG. 7. The maximum THz wave intensity and quantum conversion efficiency versus pump intensity I_p for $s \to f+s$ in the xz plane with a pump wavelength of 1.064 μm and θ of 5°. Initial Stokes intensity $I_s = 10$ W/mm^2.

Figure 6 shows THz wave intensities versus crystal length for $s \to f+s$ with θ of 5° in the xz plane with different pump intensities. The maximum intensities are 0.016, 0.042, 0.072, 0.10 and 0.14 MW/mm^2 when pump intensities are 10, 20, 30, 40 and 50 MW/mm^2, respectively, corresponding to the quantum conversion efficiencies of 35%, 47.1%, 53.4%, 57.7% and 61.4%. Both the maximum intensities and quantum conversion efficiencies increase with the increase of the pump intensities. The optimal crystal length corresponding to the maximum intensity decreases with the increase of the pump intensities.

Figure 7 shows the relationship among the maximum THz wave intensity, the quantum conversion efficiency and the pump intensity for $s \to f+s$ with θ of 5° in the xz plane. The figure demonstrates that the maximum THz intensity and quantum conversion efficiency increase with the pump intensities. THz wave with a maximum intensity of 1.1 MW/mm^2 are generated as pump intensity equals 30 GW/cm^2 which is the optical damage threshold of KTP, corresponding to the quantum conversion efficiency of 81.8%.

The high quantum conversion efficiencies of SPS result from the following reasons. First, CPM conditions are satisfied. Second, absorption coefficients of THz waves are small for $s \to f+s$ with $\theta < \Omega$ and $s \to f+f$ with $\theta > \Omega$ in the xz plane. Third, effective nonlinear coefficients are large as ionic and electronic nonlinearities are taken into account. Fourth, high pump intensities can stimulate SPS when the optical damage threshold of KTP is high enough.

THz wave generation with SPS in KTP shows superior performance in comparison to $LiNbO_3$ and $LiTaO_3$. First, CPM cannot be realized in $LiNbO_3$ and $LiTaO_3$, whereas it can be realized in KTP. Second, effective nonlinear coefficients and parametric gain coefficients of KTP are larger than those in $LiNbO_3$ and $LiTaO_3$ [15]. Third, compared with $LiNbO_3$ and $LiTaO_3$, KTP has a higher laser damage threshold [15].

VI. CONCLUSION

CPM SPS with $s \to f+f$ in the yz plane, $s \to f+s$ with $\theta < \Omega$ in the xz plane and $s \to f+f$ with $\theta > \Omega$ in the xz plane can generate high-intensity THz waves. CPM, low absorption coefficients of THz waves, high effective nonlinear coefficients and high pump intensities enhance the intensities of THz waves. With a pump wavelength of 1.064 μm, a pump intensity of 10 MW/mm^2, an initial Stokes wave intensity of 10 W/mm^2, an optimal crystal length of 2.44 mm, THz wave intensity of 0.043 MW/mm^2 at 1.66 THz can be generated for $s \to f+f$ in the xz plane with θ of 26°, corresponding to quantum conversion efficiencies of 73%. The calculation results indicate that CPM SPS with KTP can generate THz waves with high intensities and quantum conversion efficiencies.

ACKNOWLEDGMENT

This work was supported by the National Natural Science Foundation of China (61735010 and 61601183); the Natural Science Foundation of Henan Province (162300410190); the Program for Innovative Talents (in Science and Technology) in University of Henan Province (18HASTIT023).

REFERENCES

1. K. Kawase, J. Shikata, and H. Ito, "Terahertz wave parametric source," J. Phys. D: Appl. Phys. **35**, R1-R14 (2002).
2. T. A. Ortega, H. M. Pask, D. J. Spence, and A. J. Lee, "THz polariton laser using an intracavity Mg:$LiNbO_3$ crystal with protective Teflon coating," Opt. Express **25**, 3991-3999 (2017).
3. H. Jang, G. Strömqvist, V. Pasiskevicius, and C. Canalias, "Control of forward stimulated polariton scattering in periodically-poled KTP crystals," Opt. Express **21**, 27277-27283 (2013).
4. T. A. Ortega, H. M. Pask, D. J. Spence, and A. J. Lee, "Tunable 3-6 THz polariton laser exceeding 0.1 mW average output power based on crystalline $RbTiOPO_4$," IEEE J. Sel. Top. Quantum Electron. **24**, 1-6 (2018).
5. U. T. Schwarz and M. Maier, "Damping mechanisms of phonon polaritons, exploited by stimulated Raman gain measurements," Phys. Rev. B. **58**, 766-775 (1998).
6. S. S. Sussman, *Tunable light scattering from transverse optical modes in lithium niobate*; Report No. su-mlr-1851 (1970); Microwave Laboratory, Stanford University: Stanford, CA, USA (1971).
7. T. Ikari, X. Zhang, H. Minamide, and H. Ito, "THz-wave parametric oscillator with a surface-emitted configuration," Opt. Express **14**, 1604-1610 (2006).
8. J. Kiessling, F. Fuchs, K. Buse, and I. Breunig, "Pump-enhanced optical parametric oscillator generating continuous wave tunable terahertz radiation," Opt. Lett. **36**, 4374-4376 (2011).
9. D. H. Wu and T. Ikari, "Enhancement of the output power of a terahertz parametric oscillator with recycled pump beam," Appl. Phys. Lett. **95**, 141105 (2009).
10. D. N. Nikogosyan, *Nonlinear Optical Crystals: a Complete Survey* (Springer, New York, USA, 2005).
11. F. C. Zumsteg, J. D. Bierlein, and T. E. Gier, "K_xRb_1-$_xTiOPO_4$: a new nonlinear optical material," J. Appl. Phys. **47**, 4980-4985 (1976).
12. H. Y. Zhu, G. Zhang, C. H. Huang, Y. Wei, L. X. Huang, and Z. Q. Chen, "Multi-watt power blue light generation by intracavity sum-frequency-mixing in $KTiOPO_4$ crystal," Opt. Express **16**, 2989-2994 (2008).
13. G. C. Bhar, A. M. Rudra, A. K. Chaudhary, T. Sasaki, and Y. Mori, "Highly efficient difference-frequency generation in KTP," Appl. Phys. B: Laser Opt. **63**, 141-144 (1996).
14. F. G. Colville, M. H. Dunn, and M. Ebrahimzadeh, "Continuous-wave, singly resonant, intracavity parametric oscillator," Opt. Lett. **22**, 75-77 (1997).
15. M. H. Wu, Y. C. Chiu, T. D. Wang, G. Zhao, A. Zukauskas, F. Laurell, and Y. C. Huang, "Terahertz parametric generation and amplification from potassium titanyl phosphate in comparison with lithium niobate and lithium tantalate," Opt. Express **24**, 25964-25973 (2016).
16. W. Wang, Z. Cong, X. Chen, X. Zhang, Z. Qin, G. Tang, N. Li, C. Wang, and Q. Lu, "Terahertz parametric oscillator based on $KTiOPO_4$ crystal," Opt. Lett. **39**, 3706-3709 (2014).
17. T. A. Ortega, H. M. Pask, D. J. Spence, and A. J. Lee, "Competition effects between stimulated Raman and polariton scattering in intracavity $KTiOPO_4$ crystal," in *Proc. OSA Technical Digest (online)* (Optical Society of America, 2015), paper ATu3A.3.
18. G. Kugel, F. Brehat, B. Wyncke, M. Fontana, G. Marnier, C. C. Nedelec, and J. Mangin, "The vibrational spectrum of a $KTiOPO_4$ single crystal studied by Raman and infrared reflectivity spectroscopy," J. Phys. C. **21**, 5565-5583 (1988).
19. J. G. Huang, Z. M. Huang, N. A. Nikolaev, A. A. Mamrashev, V. D. Antsygin, O. I. Potaturkin, A. B. Meshalkin, A. B. Kaplun, G. V. Lanskii, Y. M. Andreev, D. M. Ezhov, and V. A. Svetlichnyi, "Phase matching in RT KTP crystal for down-conversion into the THz range," Laser Phys. Lett. **15**, 075401 (2018).
20. C. Alberdi, J. M. Diñeiro, B. Hernández, and C. Sáenz, "General expressions for the refractive indices of absorbing biaxial media as a function of the angle of incidence," J. Opt. Soc. Am. A **32**, 228-237 (2015).
21. A. Mamrashev, N. Nikolaev, V. Antsygin, Y. Andreev, G. Lanskii, and A. Meshalkin, "Optical properties of KTP crystals and their potential for terahertz generation," Crystals **8**, 310 (2018).
22. V. D. Antsygin, A. B. Kaplun, A. A. Mamsharov, N. A. Nikolaev, and O. I. Potaturkin, "Terahertz optical properties of potassium titanyl phosphate crystals," Opt. Express **22**, 25436-25443 (2014).